Analysis of the thickness effect in thin steel welded structures under uniaxial fatigue loading

Paolo Livieri, Roberto Tovo

Department of Engineering, University of Ferrara, via Saragat 1, 44122, Ferrara

paolo.livieri@unife.it

Abstract

This paper investigates the scale effect in relatively thin welded joints subjected to fatigue loading made of steel. In the scientific literature, the fatigue behaviour of arc-welded joints is usually divided into two groups: thick and thin joints. A cut-off thickness, typically in the range of 13 mm to 22 mm, was introduced; under such cut-off value, the design fatigue strength does not increase when the thickness is decreased. Despite this common approach, in this paper, the concept of cut-off thickness is revised and a numerical procedure is proposed, regardless of the thickness of the joint, by means of the implicit gradient method. Classical non-load-carrying and load-carrying cruciform joints made of steel are considered in the three-dimensional numerical analysis. Finally, the fatigue behaviour of joints two millimetres thick with a longitudinal or transversal stiffener was also analysed by means of the implicit gradient approach. The Woehler curve was evaluated in terms of the nominal stress of such a series and a good correlation was found with experimental data by using the numerical procedure optimised for thick welded joints.

Keywords: implicit gradient, fatigue, welded joint, thickness effect, steel

2α = opening angle

c = characteristic length

E = elastic modulus

K_f = fatigue notch factor

K_{ref} = reference fatigue strength value of Notch Stress Intensity Factor (NSIF)

k = dimensionless coefficient for analytic NSIF evaluation

λ = mode I Williams' eigenvalue

N= fatigue life; cycles to failure

v= Poisson's ratio

P_s = probability of survivor

R = stress ratio

s = arc length

S = nominal fatigue strength

S_B = nominal fatigue strength from the relevant basic Woehler curve

σ_{nom} = tensile nominal stress

σ_{eff} = effective stress

$\sigma_{eff,max}$ = *maximum effective stress*

σ_{eq} = equivalent stress

σ_{uts} = ultimate tensile strength

t = thickness

t_B = cut-off thickness

Ψ = weight function

Δ = range

1. Introduction

Fatigue design rules of welded joints based on the nominal stress approach consider the scale effect by introducing a penalty function of the thickness [1,2,3]. This choice is due to experimental evidence: for a given welded detail the fatigue strength decreases by increasing the thickness, this is well documented by Gurney [4] and Maddox [5]. For example in BS 7608 [3] the thickness effect correction function is:

$$S = S_B \left(t_B / t\right)^{1/4} \qquad (1)$$

where S is the nominal fatigue strength of the joint under consideration, S_B is the fatigue strength from the relevant basic Woehler curve at a prefixed cycle to failure number N, t is the thickness of the joint and t_B is the maximum thickness related to the basic Woehler curve, equal to 16 mm for steel joints. The t_B is also considered as the *cut-off thickness* because the above equation overestimates the fatigue strength when the thickness decreases. However, as underlined by Maddox [5] and Gurney [4], the scale effect does not only depend on the thickness but also on the other dimensions. The influence of both the main plate thickness and the attachment size on the fatigue strength calculations of joints with a transverse non-load-carrying fillet weld was introduced. A different penalty function was considered and it was obtained as a function of the effective thickness or the apparent thickness of the joint dependent both on plate thickness and on the toe-to-toe length of the attachment.

From another point of view, the scale effect can be summarised as a simple relationship by means of the Notch Stress Intensity Factor (NSIF) approach [6]. When,

at the weld toe or root, the mode I loading is dominant, the nominal fatigue strength *S* of the joint under consideration can be expressed as:

$$S = K_{ref} / (k\, t^{1-\lambda}) \qquad (2)$$

where, *t* is the thickness of the joint, *k* is a dimensionless coefficient dependent only on the geometry, λ is mode I Williams' eigenvalue and K_{ref} is a reference strength value of NSIF related to a prefixed cycle to failure. Eq. (2) has been verified in many cases [6,7] and the dependence of the scale effect on Williams' eigenvalue was confirmed in Ref. [7] where the power experimental exponent resulted equal to 0.31 for toe failure (against a theoretical value of 0.33) and equal to 0.51 for root failure (against a theoretical value of 0.5).

The use of Eq. (1) for a thickness less than 16 mm was analysed in Ref. [8]. On the basis of accurate experimental results, Gurney in [8] underlined that the strength of axially loaded plates with short transverse non-load-carrying attachments given by Eq. (1) is in reasonable agreement with theoretical predictions down to a thickness of 2 mm. However, in other cases the strength for thin walled joints was not in agreement with Eq. (1) [8].

The aim of this paper is to investigate the size effects of the thickness under tensile loading by means of the implicit gradient approach in the case of cruciform steel joints. The numerical procedure optimised for thick welded joints is used without any change to the thin transverse load-carrying fillet weld and the non-load-carrying fillet weld. Finally, the fatigue life prediction curves of three thin welded joints with a longitudinal or transversal stiffener have been evaluated. All elements had a thickness of two millimetres.

2. Analytical Frame

The idea of using an average stress close to the point where failure occurs was proposed by Neuber [9] and can be generalised by considering a body of volume V and a scalar value σ_{eq} of the stress components defined all over V. On the other hand, in order to simplify the problem, the concepts of strain energy density [7, 10–12] or the critical distance approach [13, 14] consider an average in the neighbourhood of the critical point.

According to the non-local theory as proposed in Ref. [15] an effective stress σ_{eff} in the actual point P can be defined by averaging an equivalent local stress σ_{eq}, weighted by function ψ:

$$\sigma_{eff}(P) = \left(\int_V \Psi(P,Q)\, \sigma_{eq}(Q)\, dV \right) / \int_V \Psi(P,Q)\, dV \qquad (3)$$

where Q is a point inside volume V and the equivalent stress σ_{eq} is an appropriate scalar function of the stress tensor in point Q. The weight function ψ is an isotropic function of the distance $|PQ|$, which vanishes as distance $|PQ|$ increases. To overcome the evaluation of integral (3) over all the volume V, the evaluation of effective stress σ_{eff} can be substituted by a differential equation on volume V (for more details, see Refs [16]):

$$\sigma_{eff} - c^2 \nabla^2 \sigma_{eff} = \sigma_{eq} \quad \text{in} \quad V \qquad (4)$$

where *c* is a characteristic length and ∇^2 denotes the Laplacian operator. As assumed in previous papers [17–19], we have considered that *c* depends only on the material. In this paper, to solve the inhomogeneous Helmholtz equation (4), we have considered a Neumann-type boundary condition:

$$\nabla \sigma_{eff} \cdot n = 0 \quad \text{on} \quad \partial V \qquad (5)$$

where **n** is the outward normal to the boundary and the symbol ∇ indicates the gradient operator.

In the case of welded structures under fatigue loading, the stress σ_{eff} is replaced with its range. Moreover, to correctly define the equivalent stress, considering that under proportional loading the principal stress directions are constant, it is possible to define three principal stress variations at each point, by comparing the maximum and minimum values in each direction. In this paper, dealing only with proportional and mainly uniaxial loadings, the maximum principal stress variation is considered to be an appropriate choice of the equivalent stress range $\Delta\sigma_{eq}$.
In the case of multiaxial loadings, in order to improve the cycles to failure prediction, a stress-invariant based criterion should be used [19], which consists of an improvement of the well-established Crossland-like criteria already proposed in the literature [20–23].

Fig. 1 reports the scatter bands in terms of range of the effective stress σ_{eff} that is assumed independent from the shape and size of welded joints made of steel. The scatter band was established on the basis of analysis mainly due to fatigue failure of cruciform and T joints under tensile or bending loadings (see for instance reference [7] that resumes the fatigue strength of around a hundred series of welded joints).

The main plate thickness of the joints ranged from 3 mm to 100 mm with 65% of the data being relative to a thickness between 10 mm and 50 mm. The opening angle 2α was 135° for toe failure and 0° for root failure. The fatigue scatter band of Fig. 1 refers to a 2.3% and 97.7% probability of survival and the slope takes the value of 3, which is typical in steel welded structures under mode I loadings. In the Figure, the design curve of flat specimens are also reported which were obtained by means of heat

cutting [1] that is very close to 97.7% probability of survival given by the implicit gradient approach. For details similar to a heat cutting component, the effective stress exactly agrees with the nominal stress and the specimens are simply weakened by the thermal process and not by the geometrical effect due to a stress raiser.

The characteristic length parameter *c* was found to be equal to 0.2 mm [17] and is considered a property of all welded joints made of steel independent of the thickness of the main plate or attachments.

3. Numerical Analyses

The partial differential equation (4) was solved by means of COMSOL numerical finite element (FE) software, which is able to evaluate both conventional linear elastic structural analysis and the Helmholtz equation (4) by means of the same mesh. The advantage of the use of Eq. (4) is that σ_{eq} can be singular at the notch tip while the effective σ_{eff} is a continuous function all over the component. Furthermore, the effective stress is calculated in all points of the body without imposing a priori a particular critical zone by assuming the same characteristic length *c* equal to 0.2 mm [17]. All the numerical analyses were made by considering a linear elastic material with elastic modulus *E* of 200 GPa and a Poisson's ratio ν equal to 0.3 unless otherwise specified. Analytical solutions of Eq. (4) are possible, but require a previous asymptotic stress analysis that is able to evaluate the mode I notch stress intensity factors (NSIFs) of the weld [24]. In the case of spot welded joints, the implicit gradient approach proposed in Ref. [17] was used without any difficulty despite the relatively thin plate [18]. The fatigue predictions were obtained considering the weldment as a three-dimensional structure.

As an example, Fig. *2b*, shows the typical results in terms of σ_{eff} obtained by means of a numerical analysis with the three-dimensional mesh of Fig. *2a*. The welded joint is a load-carrying joint under tensile loading. A mesh with quadratic elements the size of the smaller element ranging between *c* and *c/2* is able to give a precise trend of σ_{eff} along the weld toe or root (see a convergence test in Ref. [18]). The points where the stress becomes singular are the three lines A, B and C. All these locations could be a prospective nucleation zone of a fatigue crack. However, based on the FE analysis the maximum effective stress is located at the weld root near the free-surface, so that the fatigue crack will nucleate at the root and the value of 2.6 can be considered as the fatigue notch factor K_f of the weld referred to as tensile nominal stress σ_{nom}.

3.1 Load-carrying cruciform joint

In order to analyse the thickness effect in welded joints, as a first case study, we consider a classical load-carrying joint under tensile loading that showed an experimental failure at the weld toe for a thickness of the main plate equal to 2 mm [8]. Fig. 3 shows the fatigue life prediction in terms of nominal stress against the main plate thickness at $5 \cdot 10^6$ cycles. The Figure reports the prediction in the case of failure at the toe or at the root of the weld when the shape of the joints is taken as constant. The attachment length in the direction of nominal stress is equal to 5 times the thickness of the main plate and the specimen width is equal to 75 times the thickness. The nominal stress was evaluated as a function of the thickness by imposing that the maximum effective stress will be equal to 156 MPa at $5 \cdot 10^6$ cycles for a probability of failure equal to 50% . When the thickness is greater than t^* the failure occurs at the weld root,

otherwise failure occurs at the weld toe. So that by considering the same shape of welded joints, the failure point depends on the absolute value of the thickness.
The equation of synthesis reported in Fig. 3 indicates that the scale effect of the welded notch is different if the failure occurs at the notch root or notch tip. At the weld toe where the opening angle 2α is 135° the penalty exponent is 0.31 whereas at the notch root (2α=0°) the exponent is 0.51. These values are in perfect agreement with the scale effect analysed in reference [7] in terms of Notch Stress Intensity Factors. Furthermore, the same Figure reports the scale effect obtained by means of Eq. (1) for class F2 of BS7608 related to load-carrying joints with a partial penetration butt or fillet weld with failure at the weld toe for a 50% probability to failure.

Fig. 4 reports the trend of the effective stress σ_{eff} at the weld root or at the weld toe for the thickness equal to 2 millimetres. The maximum value is at the weld toe. Because the weld can be obtained by extrusion of a two-dimensional draw, the values of σ_{eff} obtained in a two-dimensional FE analysis, are also reported. The two-dimensional analysis gives results close to those obtained in the middle of the plate.

As far as the trend of the effective stress along the transverse direction is concerned, Fig. 5 shows the comparison between the principal stress and the effective stress. The effective stress is evaluated at the weld toe because, in virtue of Eq. 5, it is defined also at the notch tip of sharp notches. In contrast, the maximum principal stress is evaluated at three different distances from the weld toe because it is singular at the tip [6]. In light of the trend of the dimensionless stresses reported in Fig. 5, it is clear that the shape of the effective stress is very similar to the shapes of the principal stress as the distance from the weld toe decreases.

As underlined by Pook in Ref. [25], the existence of three-dimensional effects for linear elastic materials at cracks and sharp notches has been known for many years, but understanding has been limited, and for some situations, it still is. In general, very accurate three-dimensional mesh is needed to explain the trend of the stress near corner

point singularities. For example, in Ref. [26–27] the influence coupled modes generated by anti-plane loading is carefully analysed. The plate/disc bending on three-dimensional stress fields was considered in the investigation, showing that it becomes non-negligible as the thickness decreases. In particular, when it is applied a remotely nominal mode III does produce a coupled mode II. Recently, Pook et al. [28] showed that the stresses in the vicinity of a corner point appear to be sums of stresses due to two different singularities of different orders: stress intensity factors and corner point singularities, but further FE analysis with a more detailed mesh is needed.

As far as load-carrying welded joints are concerned, it is clear that the drop behaviour of the σ_{eff} is related to the first principal stress as appears in Figs 4 and 5. From a numerical point of view, the analysis of the effective stress σ_{eff} requires a less detailed mesh than that in Refs [26–28] because of the integral nature of Eq. (4). A mesh with the smaller element size of the same order of c gives good results [8]. For sharp notches, at the tip, the effective stress σ_{eff} depends on all NSIFs of the weld linked to the mode I, mode II and mode III loading. From this point of view, the effective stress σ_{eff} is directly linked to the actual stress state related to the actual three-dimensional nature of the stress that is meaningful as an average value inside a volume of radius of 4–5 times c. However, for the load-carrying welded joints under nominal tensile loading it is sufficient to assume a Poisson's ratio v equal to zero to avoid the three-dimensional effects [29], as reported in Figs 4 and 5. By assuming $\nu=0$, σ_{eff} remains constant along the entire notch tip.

In order to underline the rule of the thickness, Fig. 6 reports the value of maximum effective stress ($\sigma_{eff,max}$) for different b/t ratios; with b being the width of the plate. When b/t increases the maximum values at the notch tips increase but the maximum value is always reached at the toe.

Fig. 7 shows that, if the geometry changes (attachment length in the direction of nominal stress equals 2.4 times the thickness of the main plate, indeed 5 times as in Fig. 3), the t^* turns out to be different from the previous case. For instance t^* moves from 21 to 5 mm, respectively. The penalty exponent slightly changes compared to those reported in Figure 4. The experimental data obtained by Sørensen et al. [30] confirm that for a thickness equal to 10 mm the failure is at the weld root.

3.2 Non-load-carrying cruciform joint

The analysis of a non-load-carrying cruciform joint under tensile loading is made in Fig. 8. For this type of joint, the location of maximum effective stress is always close to the weld toe. Fig. 8 shows the predictions, in terms of nominal stress, of the fatigue strength at $5 \cdot 10^6$ cycles by imposing that the maximum effective stress reaches a value of 156 MPa for a 50% probability of failure. The experimental data reported in the Figure have a dimensionless coefficient *k* close to 1.15 (for *k* see Eq.(2)) and a total attachment length around two times the main plate thickness [7]. Furthermore, the NSIF approach by means of Eq. (2), predicts these experimental data with good accuracy. These analyses were based on a two-dimensional prediction of NSIF [6, 7]. The fatigue prediction based on the implicit gradient approach takes into account a three-dimensional analysis where the attachment length in the direction of nominal stress is equal to two times the thickness of the main plate. The experimental data related to a thickness ranging between 3 and 50 mm are in agreement with the analytical prediction, however, for a thickness less than 3 mm the fatigue strength prediction with the implicit gradient begins to show a different behaviour from the NSIF approach, because the increment of the effective stress distribution when *b/t* increases. Finally, Fig. 9 reports the trend of the effective stress along the weld toe. The influence of the width *b* over the thickness *t* is clear. In the middle of the plate the value of the effective stress is close to that obtained by means of a two-

dimensional FE analysis. Usually, for the experimental results proposed in Refs [4 and 5] the *b/t* ratio for thickness equal to or greater than 25 mm ranges from 0.5–5, whereas when the thickness is around 10–13 mm the *b/t* ratio ranges from 10–15. So that, the equivalent stress obtained from a two-dimensional FE analysis of welded joints of Refs [6 and 7] is close to the maximum value evaluated by means of a three-dimensional FE analysis. Based on the results reported in Fig. 9 the difference in the maximum effective stress prediction is around a few per cent.

3.3 Specimen with simple welded joints with a thickness of two millimetres

In order to predict the fatigue behaviour of thin welded joints, now we consider three types of welded joints obtained with plates having a thickness of two millimetres. In the next three sections, the use of three-dimensional FE analysis is of fundamental importance. All experimental data were considered by Gurney [8] that give detailed information on the geometry. The nominal load ratio R was equal to zero for the tensile test, whereas in the case of the four-point bending mode, tests were carried out at a small positive stress ratio.

The prediction of the fatigue scatter band curve in terms of nominal stress has been made by applying the following procedure:

1) Evaluate the maximum effective stress $\sigma_{eff,max}$ for a reference nominal stress σ_{nom} by means of FE analysis;
2) Calculate the fatigue strength factor K_f as $\sigma_{eff,max} / \sigma_{nom}$;
3) Draw the fatigue scatter band curve by dividing the values of Fig. 1 by K_f ;

As far as the slope of the fatigue curve is concerned, the experimental data indicated that the slope it not determined only by the thickness. In fact, Sonsino et al. [31] suggested that the slope is a result of the iteration among the thickness, local geometry

structural stiffness, loading mode and residual stresses. The complexity makes it difficult to identify the driven parameter, so that, in this paper the slope of the fatigue scatter band of Fig. 1 was kept constant and equal to 3 as in a previous paper [18] where a linear elastic behaviour of material was taken into account. The joints considered in the next section are locally subjected mainly to mode I loading, so that a slope equal to 3 can be appropriate because the experimental data used for the assessments of Fig. 1 were subjected mainly to mode I loading [7]. If a multiaxial model is introduced, the slope can change from 3 to 5 (see paper [19] for details), which may also change by introducing a non-linear model for the material [32].

3.3.1 Longitudinal non-load-carrying fillet weld

Fig. 10 shows a longitudinal non-load-carrying fillet weld subjected to a tensile loading with thickness t=2 mm. Due to symmetries of the model, only a quarter of the plate has been analysed. The trend of the effective stress σ_{eff} in dimensionless form is reported in Fig. 11. The maximum value of effective stress occurs at the point A due to the stress concentration given by the longitudinal plates. By moving along the weld toe the stress concentration rapidly decreases with the distance measured along the weld toe. The fatigue strength predictions are illustrated in Fig. 12. The experimental point falls into the scatter band related to the average value plus/minus 2 standard deviations.

3.3.2 Transverse non-load-carrying fillet weld with short attachment under tensile loading

The principal dimensions of the transverse non-load-carrying fillet weld with short attachment under tensile loading are summarised in Fig. 13. The stress analysis confirms

that the maximum effective stress is located near the end of the transverse plate as shown in Fig. 14. If a zero Poisson's ratio is considered in the analysis, the effective stress preserves a drop after point B. In this case the stiffness of the short attachment modified the transversal contraction. Note that, the NSIF is not defined in point A, whereas the effective stress can be defined in every point of the body.

Also in this case, the experimental points fall inside the predicted fatigue scatter band reported in Fig. 15.

3.3.3 Transverse non-load-carrying fillet weld with short attachment under bending loading

As with the last case study, the effect of bending was taken into account. The principal dimensions of the transverse non-load-carrying fillet weld with a short attachment are reported in Fig. 16. The prediction of the fatigue curves in terms of nominal stress is shown in Fig. 17. As underlined by Gurney, all specimens were tested at nominal stresses above 0.2% proof stress of the material (157 MPa). Despite this high stress level, the points fall into the scatter band evaluated by imposing a linear elastic behaviour of the material.

4. Conclusions

The implicit gradient approach simplified the fatigue strength assessment of arc welded joints. By means of a single numerical procedure, based on the linear elastic behaviour of the material, different welded joints can be analysed without dividing the welded structures into thin and thick joints. A three-dimensional analysis of the weld has fundamental importance. A continuous variation of fatigue strength turned out, as a function of the thickness of the main plate. In general, there was a very good agreement between the theoretical and experimental fatigue strength also when considering only a few millimetres in thickness.

By means of the implicit gradient approach for load-carrying welded joints, it is even possible to distinguish when the failure occurs at the root or at the toe and their sensitivity to main thickness is different. The numerical analysis shows that the fatigue failure moves from weld toe to weld root as a function of the main plate thickness and the transition plate thickness depends on the weld joint shape. The exponent of the scale effect is different if failure occurs at the notch tip or notch root, depending on the analysis based on the NSIF approach.

The three-dimensional effects related to the increasing of the effective stress near the free-surface seem to be due to a combined action of the Poisson’s ratio and of the increasing stiffness due to the transverse plate and fillet welds.

References

[1] Eurocode 3: Design of steel structures; General rules. 1993-1-1

[2] A.F. Hobbacher, Fatigue design of welded joints and components, Recommendations of IIW, XIII-XV XIII-1539-96/XV-845-96, 1996, ABINGTON PUBLISHING

[3] British Standard Published Document, Code of practice for fatigue design and assessment of steel structures, BS 7608, 1993

[4] T.R. Gurney, (1991). The fatigue strength of transverse fillet welded joints. Abington Publishing, Cambridge.

[5] S.J. Maddox, (1995). Scale effect in fatigue of fillet welded aluminium alloys. Proc. Sixth International Conference on Aluminium Weldments, Cleveland, Ohio, pp 77–93

[6] P. Lazzarin, R. Tovo, (1998). A Notch Intensity Approach to the Stress Analysis of Welds. Fatigue and Fracture of Engineering Materials and Structures 21, pp 1089–1104

[7] P. Livieri, P. Lazzarin, (2005), Fatigue strength of steel and aluminium welded joints based on generalised stress intensity factors and local strain energy values, *International Journal of Fracture*, 133, pp 247–376

[8] T.R. Gurney, (1997). Fatigue of thin walled joints under complex loading. Abington Publishing, Cambridge.

[9] H. Neuber, Uber die Berucksichtigung der Spannungskonzentration bei Festigkeitsberechnungen. Konstruktion 1968; 20 (7): 245–51

[10] P. Lazzarin, R. Zambardi, A finite-volume-energy based approach to predict the static and fatigue behavior of components with sharp V-shaped notches. Int J Fract 2001;112:275–98

[11] F. Berto, P. Lazzarin: A review of the volume-based strain energy density approach applied to V-notches and welded structures, Theoretical and Applied Fracture Mechanics, Volume 52, Issue 3, December 2009, Pages 183–194

[12] P. Lazzarin, F. Berto, F.J. Gomez, M. Zappalorto, Some advantages derived from the use of the strain energy density over a control volume in fatigue strength assessments of welded joints, *International Journal of Fatigue*, *Vol. 30, 8*, *2008*, *pp 1345–1357*

[13] D. Taylor, (1999) Geometric effects in fatigue: a unifying theoretical model. *International Journal of Fatigue* 21, 413–420

[14] L. Susmel, D. Taylor. The Theory of Critical Distances to estimate lifetime of notched components subjected to variable amplitude uniaxial fatigue loading, *International Journal of Fatigue*, *Vol. 33, 7*, *2011*, *900–911*

[15] G. Pijaudier-Cabot and Z.P. Bažant, Nonlocal Damage Theory (1987), *Journal of Engineering Mechanics*, 10 pp 1512–1533

[16] R.H.J. Peerlings, R. de Borst, W.A.M. Brekelmans, J.H.P. de Vree, (1996), Gradient enhanced damage for quasi-brittle material. *International Journal of Numerical Methods in Engineering* 39, pp 3391–3403

[17] R. Tovo, P. Livieri, (2007) An implicit gradient application to fatigue of sharp notches and weldments. *Engineering Fracture Mechanics* 74, pp 515–526

[18] R. Tovo, P. Livieri, (2010) A numerical approach to fatigue assessment of spot weld joints. Fatigue and Fracture of Engineering Materials and Structures, Volume 34, Issue 1, pp 32–45

[19] A. Cristofori, P. Livieri, R. Tovo, An implicit gradient application to fatigue of sharp notches and weldments, International Journal of Fatigue 31 (2009) 12–19

[20] A. Cristofori, L. Susmel, R. Tovo: A stress invariant based criterion to estimate fatigue damage under multiaxial loading, Int J Fatigue, 2008, accepted for publication.

[21] B. Crossland, Effect of large hydroscopic pressures on the torsional fatigue strength of an alloy steel. In: Proceedings of international conference on fatigue of metals, London, New York; 1956. pp 138–49

[22] B. De Freitas Li, M. De Freitas, A procedure for fast evaluation of high-cycle fatigue under multiaxial random loading. J Mech Design 2002;124:558–63

[23] B. Li, J.L. Santos, M. De Freitas, A computerized procedure for long-life fatigue assessment under complex multiaxial loading. Fatigue Fract Eng Mater Struct 2001;24:165–77

[24] R. Tovo, P. Livieri, An implicit gradient application to fatigue of complex structures, Engineering Fracture Mechanics, 75 (7), 2008, pp 1804–1814

[25] L.P. Pook, A 50-year retrospective review of three-dimensional effects at cracks and sharp notches. Fatigue Fract. Engng. Mater. Struct. 2013, 36(8), 699–723

[26] A. Kotousov, P. Lazzarin, F. Berto and L.P. Pook, Three-dimensional stress states at crack tip induced by shear and anti-plane loading. Eng. Fract. Mech. 2013, 108, 65–74

[27] L.P. Pook, F. Berto and A. Campagnolo, Coupled fracture modes of discs and plates under anti-plane loading and a disc under in-plane shear loading. Fatigue Fract. Engng. Mat. Struct. 2016, 39(8), 924–938.

[28] L.P. Pook, F. Berto and A. Campagnolo, State of the art of corner point singularities under in-plane and out-of-plane loading. Eng. Fract. Mech. In press

[29] P. Livieri, G. Nicoletto: Elasto-Plastic Strain Concentration Factors in Finite Thickness Plates, The Journal of Strain Analysis for Engineering Design, 2003, Vol. 38(1), pp 31–36

[30] J.D. Sørensen, J. Tychsen, J.U. Andersen, R.D. Brandstrup, (2006) Fatigue Analysis of Load-Carrying Fillet Welds Journal of Offshore Mechanics and Arctic Engineering, Vol. 128, pp 65–74

[31] C.M. Sonsino, T. Bruder, J. Baumgartner, S-N Lines for Welded Thin Joints — Suggested Slopes and FAT Values for Applying the Notch Stress Concept with Various Reference Radii, Weld. World. 54 (2010) R375–R392.

[32] P. Livieri, E. Salvati, R. Tovo, A non-linear model for the fatigue assessment of notched components under fatigue loadings *International Journal of Fatigue*, *Volume 82, Part 3*, *January 2016*, *pp 624–633*

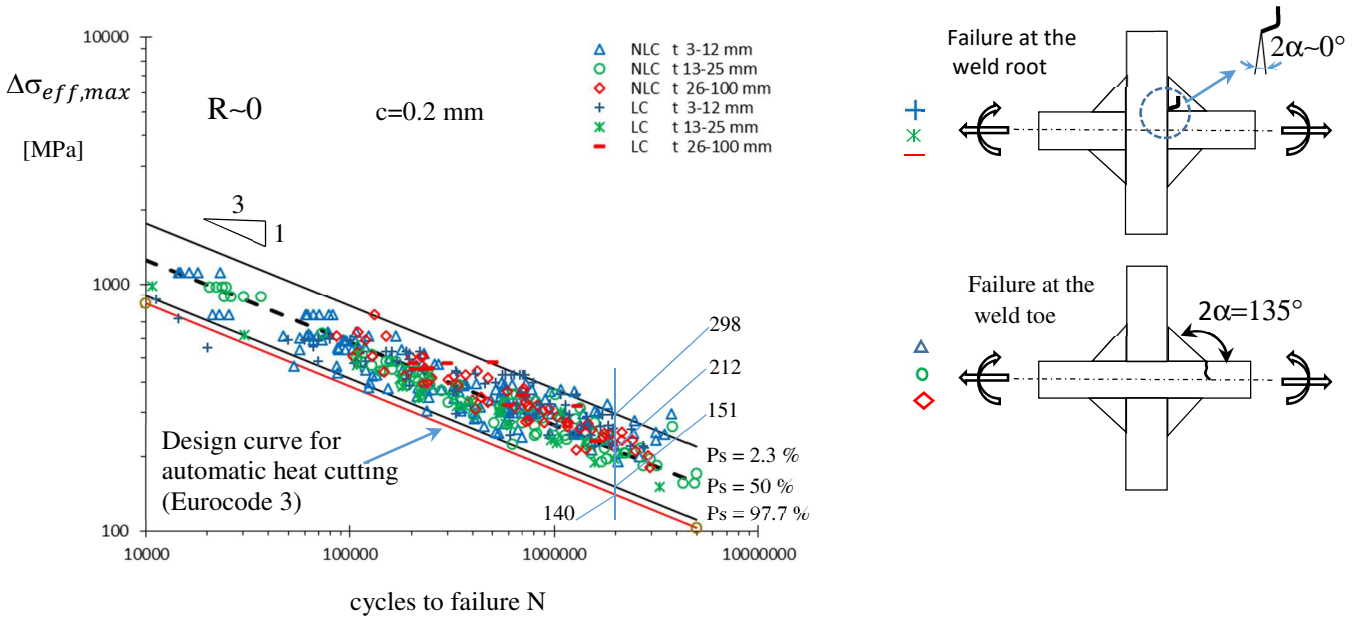

Fig. 1. Scatter band of steel welded joints in terms of maximum effective stress range (scatter bands related to mean values plus/minus 2 standard deviations; NLC: non-load-carrying joint, LC: load-carrying joint)

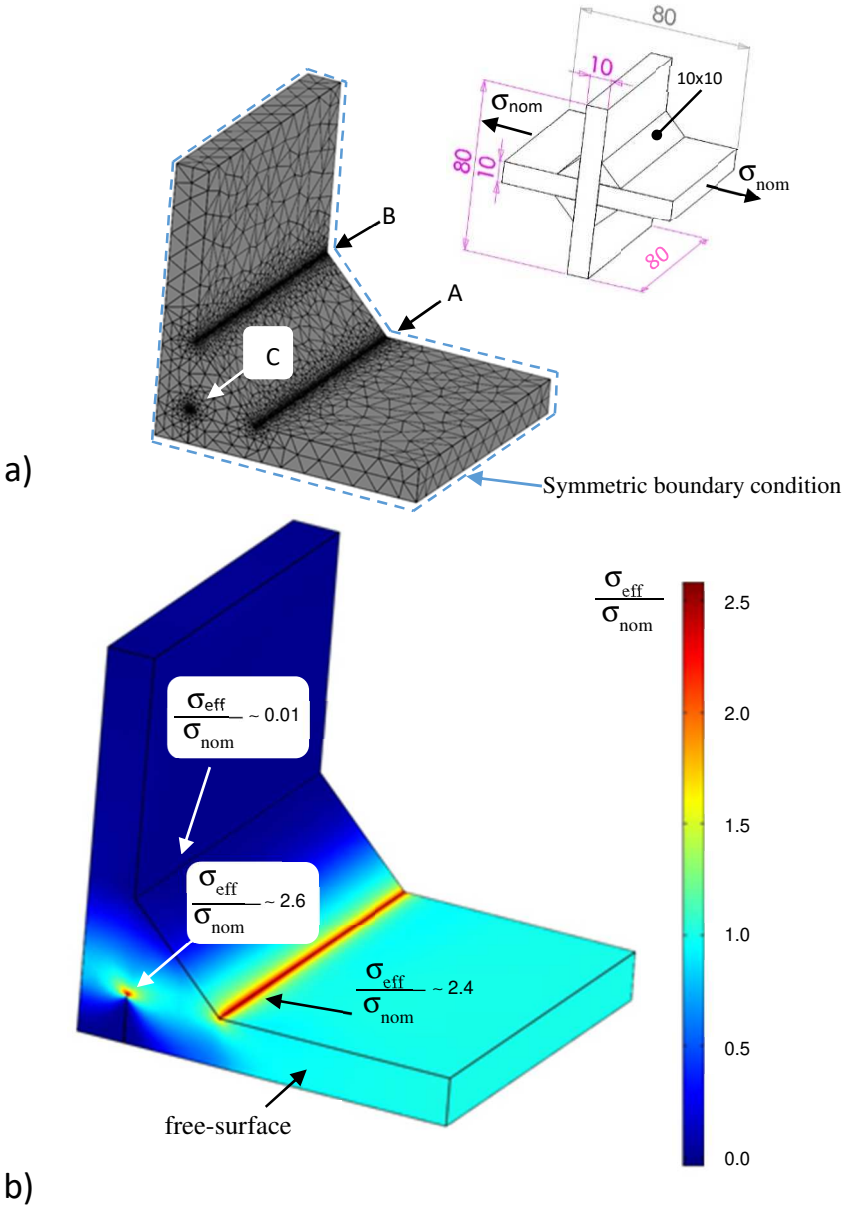

Fig. 2. a) Mesh used in the FE analysis for a load-carrying joint (the flank angle was of 135°; all dimensions are in millimetres, the minimum size of the elements is around 0.2 mm); b) effective stress σ_{eff} relate to a nominal tensile stress σ_{nom} (c=0.2 mm)

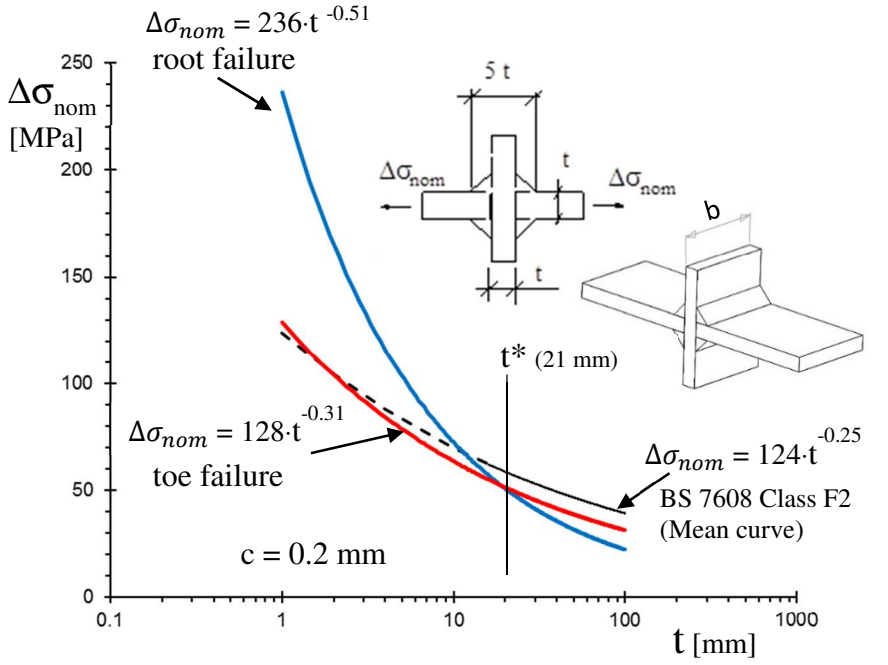

Fig. 3. Failure prediction for a load-carrying welded joint with a fixed shape as a function of the main plate thickness *t* (width *b* equal to 75·*t* and flank angle was 135° (N=5·10^6 cycles to failure, 50% probability of failure, the dashed line is the prediction by means of BS 7608 for a thickness less than the cut-off thickness)

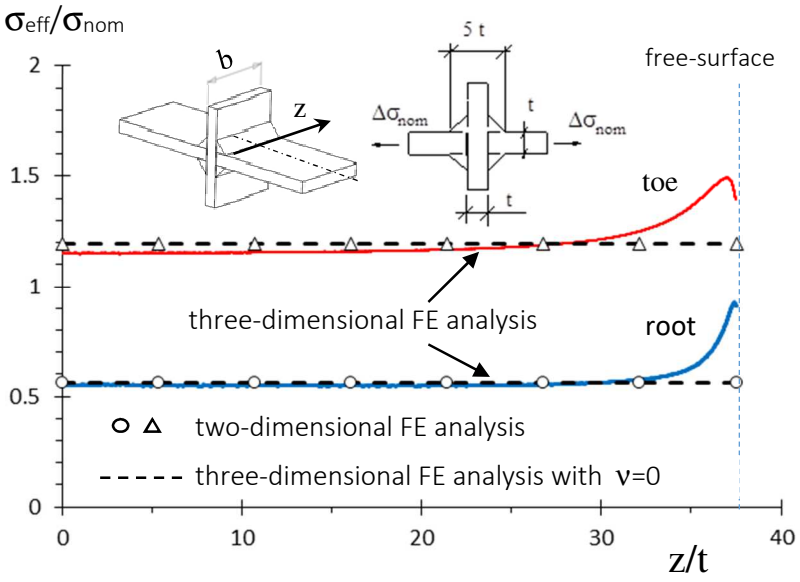

Fig. 4. Trend of the effective stress at the weld root and weld toe for a load-carrying welded joint with a thickness *t* of 2 mm (width *b* of 150 mm and a flank angle of 135°; *z* is the distance from the longitudinal symmetry plane; *c*=0.2 mm)

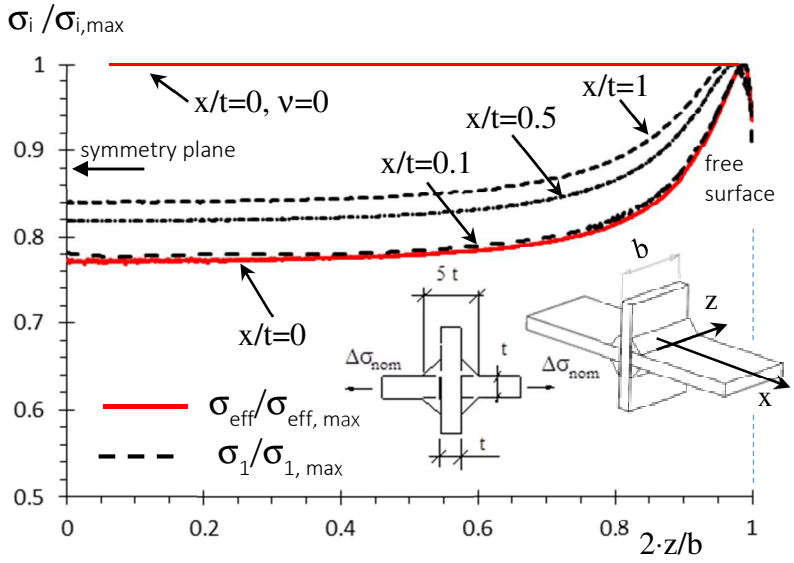

Fig. 5. Trend of the principal stress or effective stress along the transversal direction for a load-carrying welded joint with a thickness *t* of 2 mm (width *b* of 150 mm and a flank angle of 135°; *z* is the distance from the longitudinal symmetry plane, *x* is the distance from the weld toe; *c*=0.2 mm)

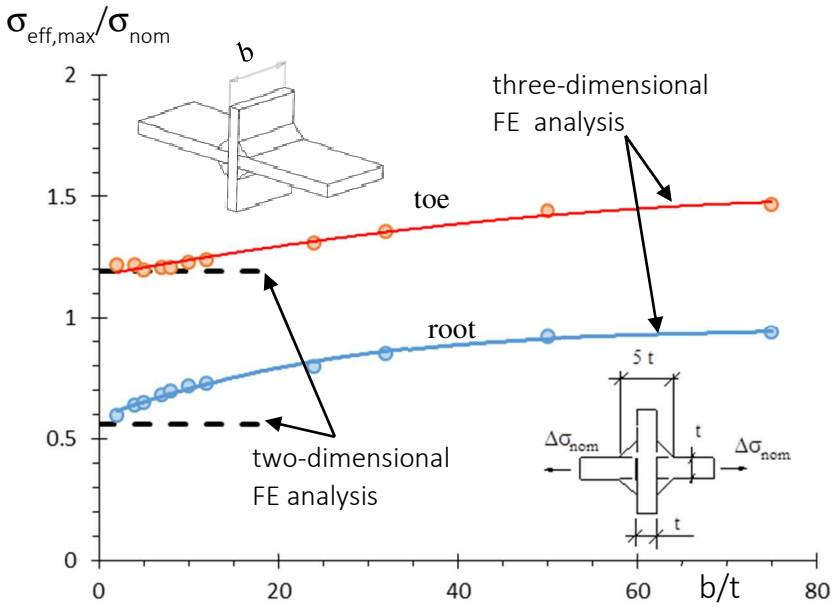

Fig. 6. Trend of the maximum equivalent stress $\sigma_{eff,max}$ at the weld root or at the weld toe for a load-carrying welded joint as a function of the dimensionless weight b/t (flank angle equal to 135°, *t= 2 mm*, *c*=0.2 mm)

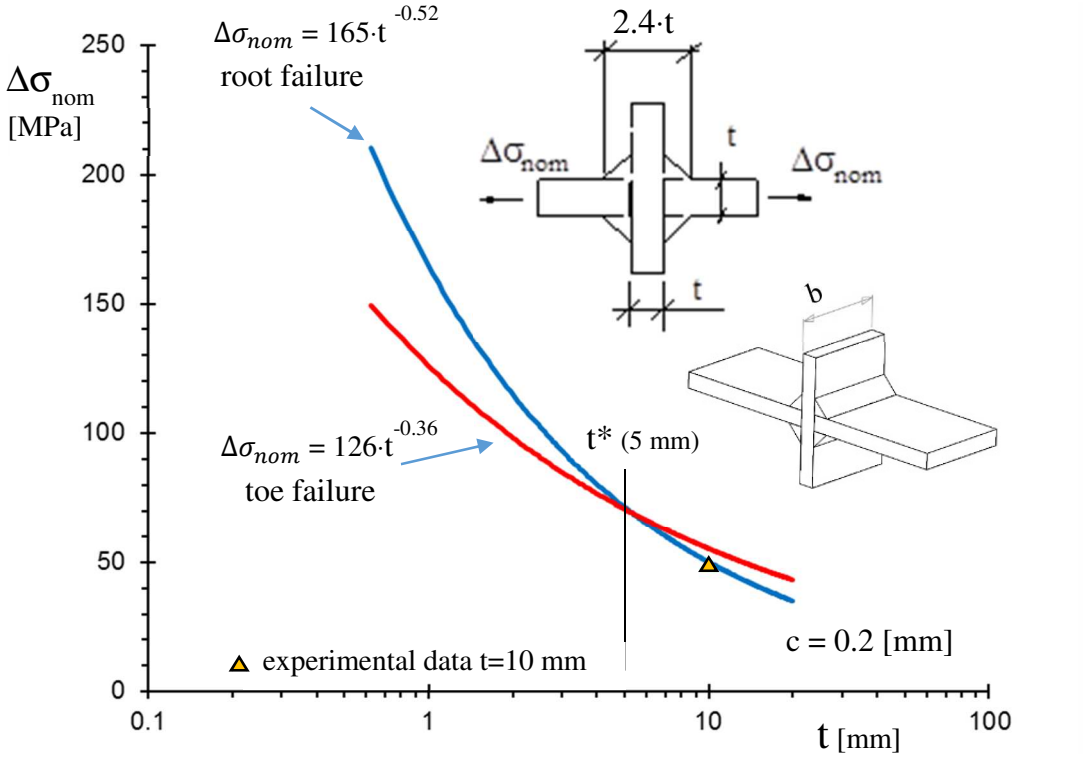

Fig. 7. Failure prediction for a load-carrying welded joint. Width *b* equal to 10·t and flank angle of 135° (experimental data from [30], N=5·10^6 cycles to failure, 50% probability of failure)

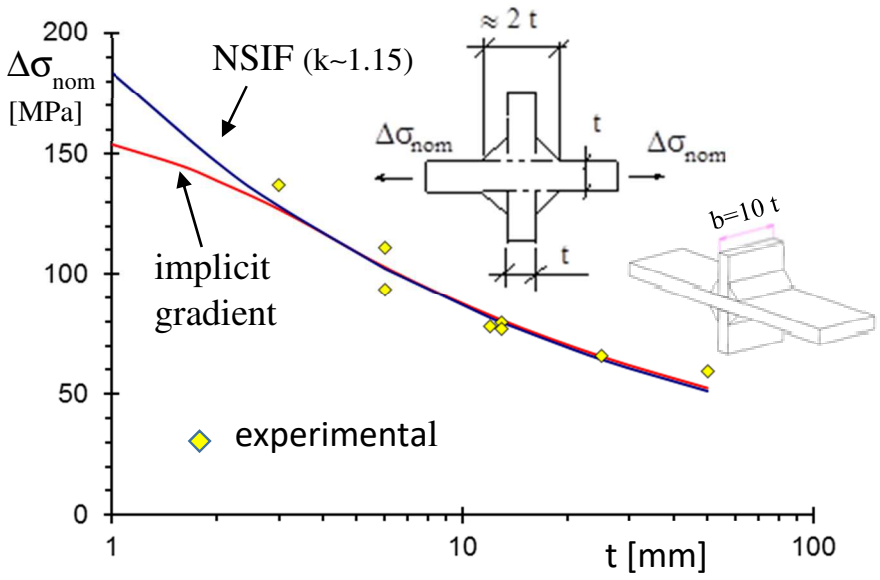

Fig. 8. Failure prediction for a non-load-carrying welded joint (for experimental data the dimensionless coefficient *k* is close to 1.15 [7], N=5·10^6 cycles to failure, 50% probability of failure). For the implicit gradient approach, the width *b* is equal to 10·t and flank angle is 135°, *c*=0.2 mm)

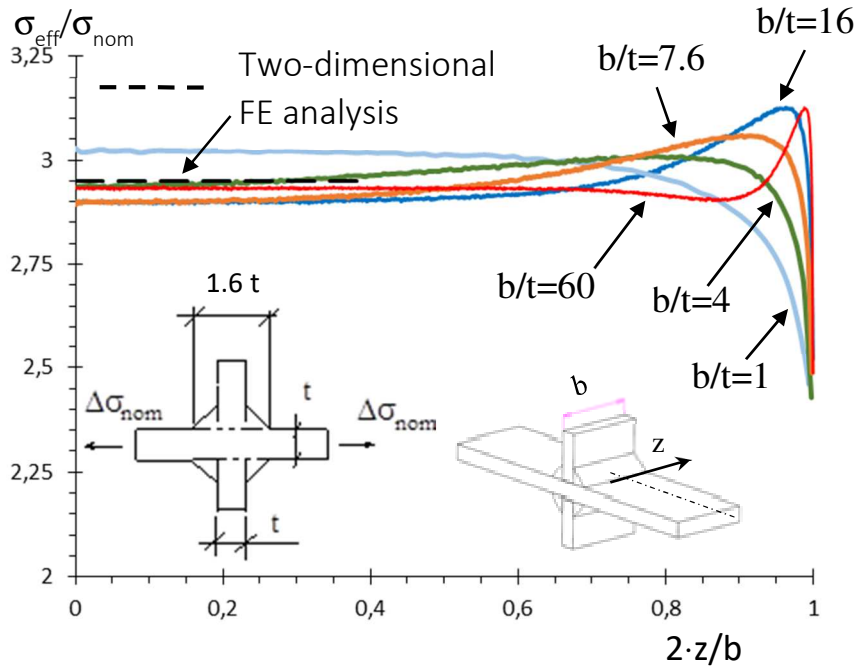

Fig. 9. Trend of the effective stress at the weld toe for a non-load-carrying welded joint with a thickness *t* of 50 mm and a flank angle of 135° (*z* is the distance from the longitudinal symmetry axis, *c*=0.2 mm)

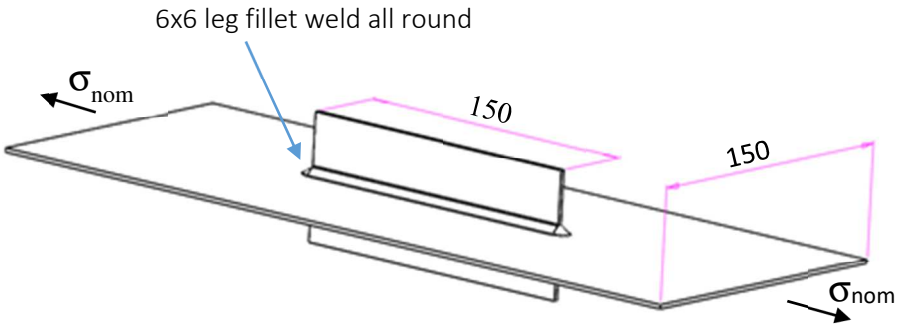

Fig. 10. Longitudinal non-load-carrying fillet weld under tensile loading. Plate thickness 2 mm (data from [8])

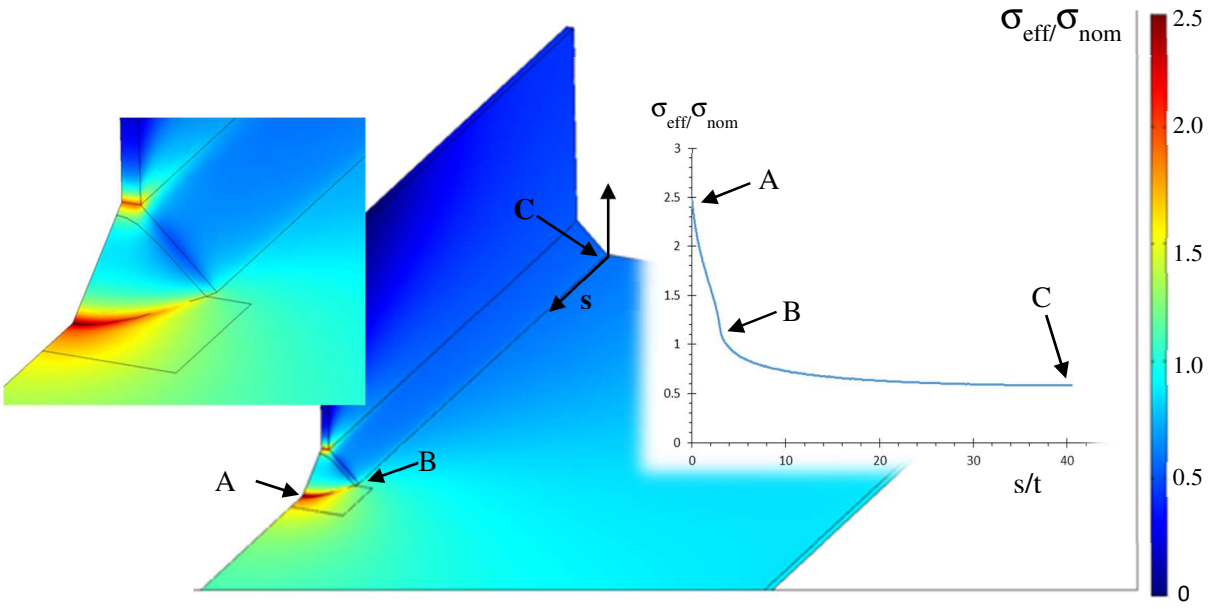

Fig. 11. Effective stress in dimensionless form for the longitudinal non-load-carrying fillet weld of Fig. 10 under tensile loading. s is the arc length along the weld toe (c=0.2 mm).

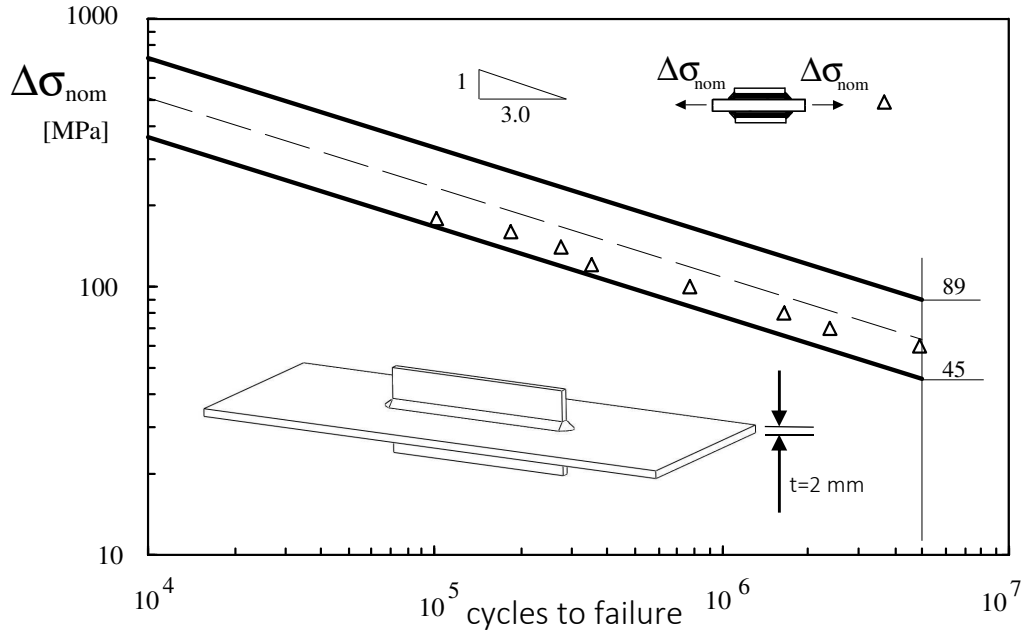

Fig. 12. Fatigue curves prediction in terms of nominal stress for the longitudinal non-load-carrying fillet weld of Fig. 10. The scatter band is related to the average value ± 2 standard deviations (experimental data from [8], R=0.1, *c*=0.2 mm)

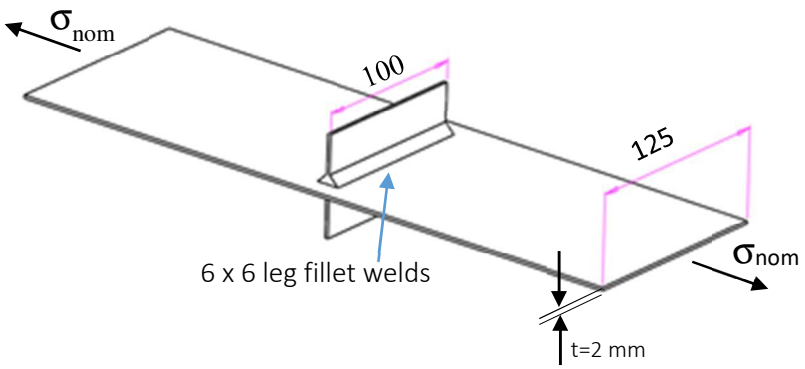

Fig. 13. ***Transverse non-load-carrying fillet weld with short attachment under tensile loading***. Plate thickness 2 mm (data from [8]).

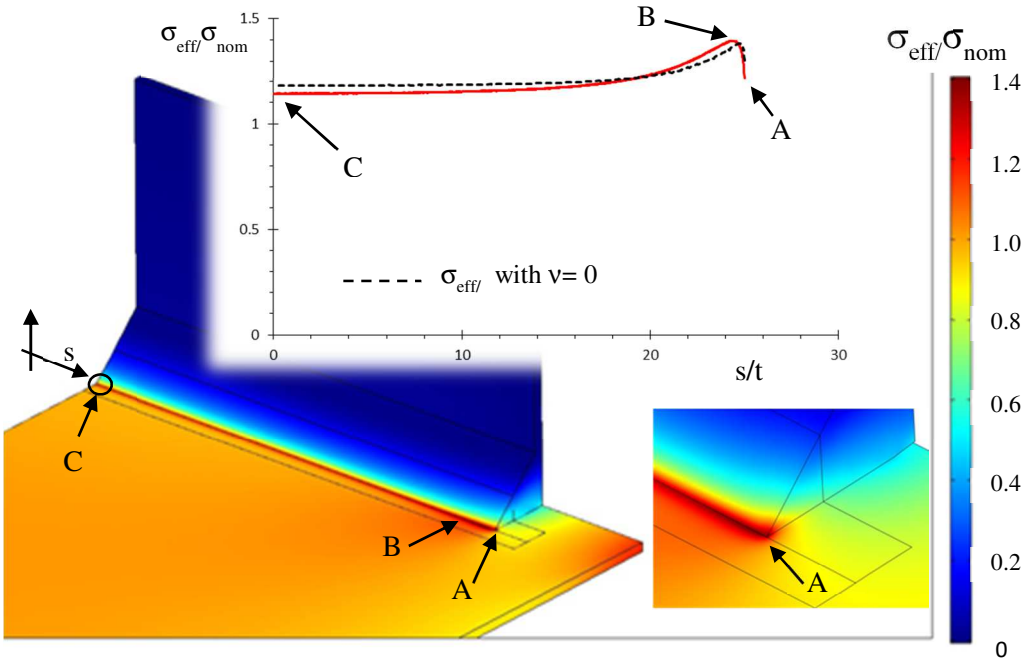

Fig. 14. Effective stress in dimensionless form for the ***transverse non-load-carrying fillet weld with short attachment under tensile loading*** of Fig. 13. s is the arc length along the weld toe with the origin at point *C belonging to the longitudinal symmetry axis* (*c*=0.2 mm)

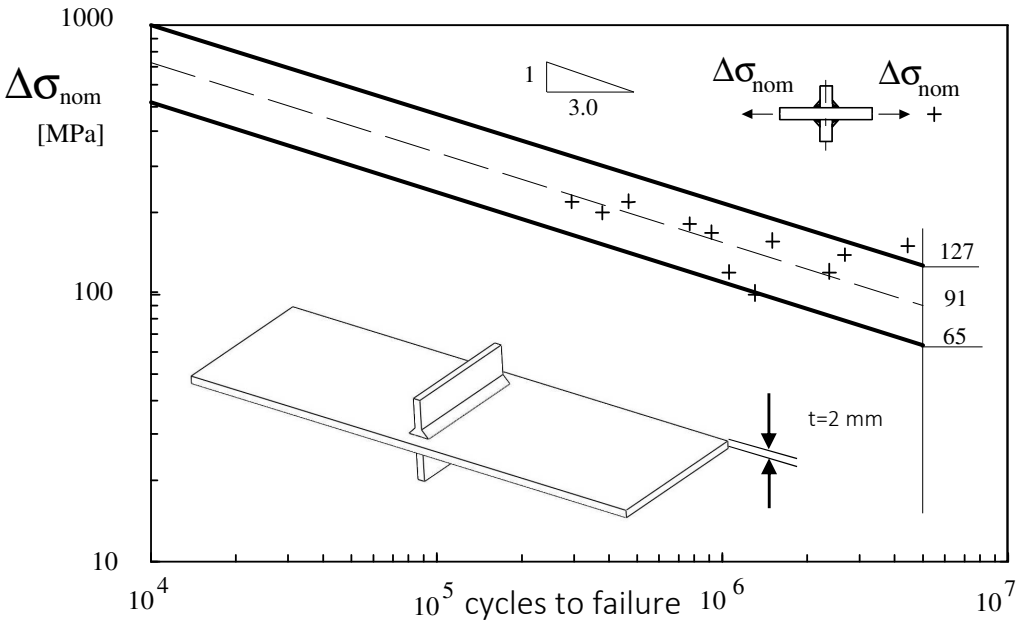

Fig. 15. Fatigue curve prediction in terms of nominal stress for the transverse non-load-carrying fillet weld of Fig. 13. The scatter band is related to the average value ± 2 standard deviations (experimental data from [8], R=0.1, *c*=0.2 mm)

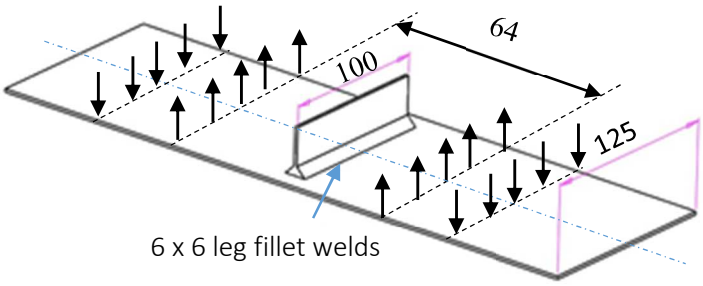

Fig. 16. ***Transverse non-load-carrying fillet weld with short attachment under four point bending***. Plate thickness 2 mm (data from [8])

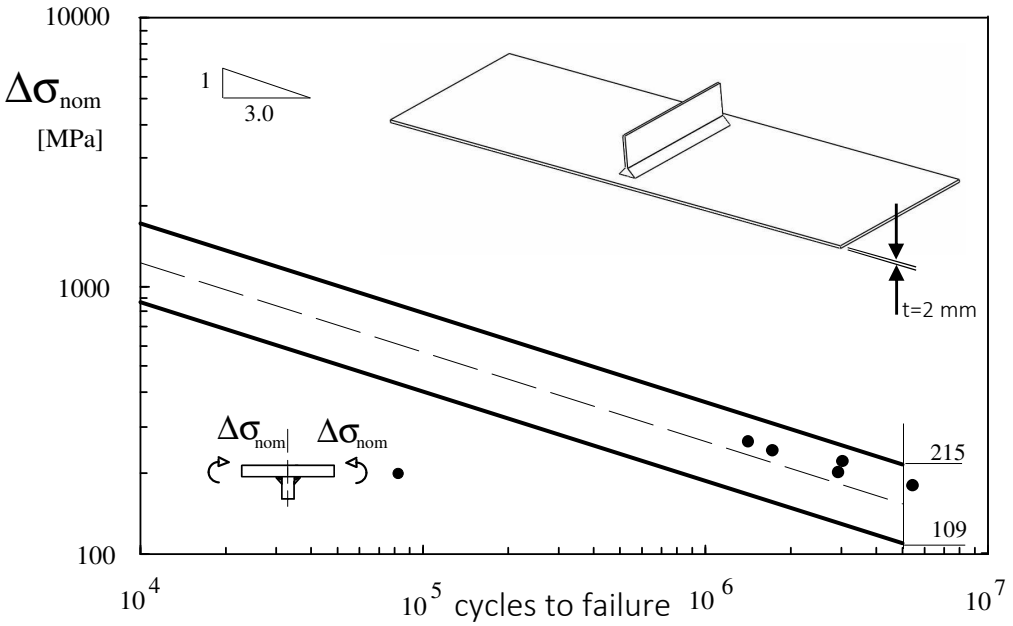

Fig. 17. Fatigue curves prediction in terms of nominal stress for the transverse non-load-carrying fillet weld of Fig. 16. The scatter band is related to the average value ± 2 standard deviations (experimental data from [8], R=0.1, *c*=0.2 mm)